Applied Organometallic Chemistry

WILEY

Applied Organometallic Chemistry

RESEARCH ARTICLE OPEN ACCESS

The Amyloid Beta Aggregation Inhibition Properties of New Pt (II) Complexes and Their Potential in Alzheimer's Treatment

Salih Günnaz[1] | Onur Şahin[2] | Sevil İrişli[1]

[1]Department of Chemistry, Faculty of Science, Ege University, Izmir, Turkey | [2]Department Occupational Health and Safety, School of Health, Sinop University, Sinop, Turkey

Correspondence: Sevil İrişli (sevil.irisli@ege.edu.tr)

Received: 5 March 2025 | **Revised:** 28 March 2025 | **Accepted:** 31 March 2025

Keywords: anti-Alzheimer activity | benzimidazole | platinum complexes | Schiff base

ABSTRACT

In this study, N-phenylortho-phenylenediamine and N-phenyl ethylenediamine were utilized as amines, and two novel ligands, benzimidazole (LI) and Schiff base (LII), were synthesized through condensation reactions with 3-methoxy-4-benzyloxybenzaldehyde. Furthermore, using these same amines, LIII (benzimidazole) with 3-phenoxybenzaldehyde and LIV (Schiff base) with 4-benzyloxybenzaldehyde were synthesized in accordance with the literature. Then, Pt (II) complexes (Ia, Ib, II, III, and IV) were prepared with these ligands, and it was determined that Ia and Ib are geometric isomers. The ligands and complexes were characterized using ^{1}H-NMR, ^{13}C-NMR, FT-IR, and elemental analysis methods. The cytotoxic effects of these complexes were evaluated on SH-SY5Y neuronal cells. Low-toxicity complexes Ia, II, and IV were then tested for their ability to inhibit amyloid beta ($A\beta_{1-42}$) aggregation. Thioflavin T fluorescence analysis, AFM imaging, and MALDI-TOF mass spectrometry demonstrated that these complexes, particularly at a 1:1 complex-to-amyloid molar ratio, effectively inhibited Aβ aggregation. These findings suggest that Pt (II) complexes containing Schiff base and benzimidazole ligands may be effective against Alzheimer's disease by alleviating Aβ toxicity.

1 | Introduction

Neurodegenerative diseases (NDs) are chronic and progressive disorders. One of these diseases, Alzheimer's disease (AD), which causes damage and memory loss by the accumulation of protein aggregates in certain areas of the brain [1, 2], leads to cognitive decline, behavioral disturbances, and loss of abilities. As a result, AD is a long-term neurodegenerative disorder that negatively affects patients' ability to function socially [3, 4]. Although there are multiple factors that cause AD, the most prominent factor is the accumulation of amyloid (specifically $A\beta_{1-42}$). This accumulation leads to the formation of senile plaques with the formation of oligomers, protofibrils, and fibrils, ultimately causing the aforementioned behavioral disorders [5, 6]. It is known that some prodrugs (ligands) used to alleviate the symptoms of AD contain some pharmacophore groups containing nitrogen atoms [7, 8]. The main aim in these applications has been to prevent the binding of ions such as Cu, Zn, and Al, which contribute to the cumulative accumulation of $A\beta_{1-42}$. However, consideration of metal complexes that may bind instead of ions such as Cu, Zn, Al has led to the formation of a hypothesis called the metal ion hypothesis, and studies using some metal complexes have emerged [9–11].

With the discovery of cisplatinum by Rosenberg in 1965 and its use in the treatment of cytotoxic tumors and the increasing

importance of Pt (II) complexes, researchers turned to the synthesis of Pt complexes in studies investigating the effects of new prodrugs. Analogous platinum (II) coordination compounds have been synthesized to investigate their effects in AD, and the ligands used in these complexes are generally ligands containing N-donor atoms [12–17]. The studies by one group of researchers of complexes that can prevent Aβ aggregation by binding to histidine residues (His6, His13, and His14) near the N-terminal region of the Aβ peptide are seminal studies in this area. The researchers synthesized Pt complexes containing nitrogen donors such as 1,10-phenanthroline and bypyridine and investigated their potential ability to inhibit Aβ aggregation. They predicted that the synthesized metal complexes would modulate Aβ aggregation and toxicity resulting from binding to the histidine residues of amyloid by separating the unstable Cl groups [18–22]. Although such an interaction has been frequently reported in the literature for transition metal complexes, another mechanism of interaction with amyloid is the hydrolysis/solvolysis mechanism [23]. In this mechanism, metal complexes act as peptide chain breakers [24–26]. In this mechanism, amyloid is cleaved at specific sites and the complex binds to the cleaved amyloid sequences [27, 28].

Two classes of nitrogen donor ligand that have gained significant renown are Schiff bases and imidazole/benzimidazole ligands. The synthesis of these ligands is accomplished through the condensation reactions of aldehydes and amines. It is noteworthy that Schiff bases, imidazole/benzimidazole ligands, and their metal complexes exhibit a diverse array of biological activities. These compounds have found widespread application in a variety of biological fields, including anticancer, anti-inflammatory, antifungal, antagonist, antioxidant, antimicrobial, antihelminthic, and antiulcer activities [2, 3, 12, 29–50]. However, to date, the research community has conducted only a limited number of studies on platinum complexes containing Schiff base and imidazole/benzimidazole ligands at the same time on AD [51–59].

The objective of this study was to compare the effects of Schiff base/benzimidazole-platinum complexes on AD. To the best of the knowledge of the authors, no literature data have been published that makes such a comparison. The synthesis of Schiff bases and benzimidazoles was accomplished through the utilization of two distinct amines and a singular aldehyde. For this purpose, the synthesis of one benzimidazole (LI) and one Schiff base (LII) ligand was carried out. These ligands were synthesized as a result of the condensation reactions of the same aldehyde and two different amines. The synthesis of Pt (II) complexes (Ia, Ib, and II) was then undertaken, with Ia and Ib complexes determined to be geometric isomers of each other. The structures of the synthesized ligands and complexes were elucidated by ^{1}H-NMR, ^{13}C-NMR, FT-IR, and elemental analysis. The L III and L IV ligands included in this study and the Pt complexes III and IV of these ligands were synthesized by our group and their structures were previously reported [57, 58]. The aim of the present study was to determine the cytotoxicities of the complexes and complexes III (formed with benzimidazole ligand [LIII]) and IV (formed with L IV ligand), which were previously synthesized by our group, on SH-SY5Y neuronal cells. The results obtained showed that the complexes Ib and III exhibited high toxicity. Consequently, the inhibitory properties of complexes Ia, II, and IV on the toxicity of amyloid beta were examined using a variety of methods.

2 | Experimental

2.1 | Chemicals

Reagents 4-benzyloxybenzaldehyde, 3-Methoxy-4-Benzyloxy benzaldehyde, N-phenylethylenediamine, 3-phenoxybenzaldehyde, $Na_2S_2O_5$, CH_3OH, CH_3Cl, $(C_2H_5)_2O$, C_3H_7NO, CH_2Cl_2, C_2H_3N, C_3H_6O were purchaced from Sıgma and Merck company. Pt $(DMSO)_2Cl_2$, used as starting complex, was synthesized according to literature data [60].

2.2 | Instrumentation

2.2.1 | Structural Analysis

The infrared spectra of ligands and complexes were recorded using a Perkin Elmer Spectrum 100 Fourier transform infrared (FT-IR) spectrophotometer in the range of 400–4000 and 200–4000 cm^{-1}, respectively. ^{1}H- and ^{13}C-NMR spectra were obtained using a Varian AS 400 MHz spectrometer. $CDCl_3$, DMSO-d_6, and D_2O were used as the solvents, and tetramethylsilane was used as the internal standard. Lipophilicity measurements were conducted using a Perkin Elmer Lambda 35 ultraviolet–visible (UV–Vis) spectrophotometer. ThT measurements were performed using a Thermo Fisher Scientific Varioskan Flash microplate reader (temperature = 37°C) with the excitation and emission wavelengths of 480 and 484 nm, respectively. For AFM measurements, the device was used with Bruker Dimension Edge ScanAsyst at Ege University MATAL center. MALDI–TOF analyses were performed using a Bruker Daltonics MALDI–TOF–Autoflex III smart beam MALDI–TOF/TOF MS device.

2.2.2 | X-Ray Structure Determination

A pale yellow, single crystal of compound complex III was obtained by a slow diffusion of a 1:3 dichloromethane/hexane system at room temperature. Intensity data for complex 2 were collected on a Bruker APEX-II CCD diffractometer using graphite-monochromated Mo K α radiation (λ = 0.71073 Å) at 110 K. The structure was solved by direct methods using SHELXS-2013 [61] and refined by full-matrix least-squares methods on F 2 using SHELXL-2013 [62]. The following procedures were implemented in our analysis: data collection: Bruker APEX2 [63] a program used for molecular graphics were as follows: MERCURY programs [64]; software used to prepare material for publication:WinGX [65]. Atomic coordinates, bond lengths, and angles were deposited in the Cambridge Crystallographic Data Center, 12 Union Road, Cambridge CB2 1EZ, UK Crystal data, and the structure refinement details of complex III (**CCDC number is 2027758)** are given in Table 1.

TABLE 1 | Crystallographic data for complex III.

Parameter	Value
Molecular formula	$C_{27}H_{24}Cl_2N_2O_2PtS$
Molecular weight (Mr)	706.53 g/mol
Crystal system	Triclinic (P1)
Z (formula units)	2
Unit cell volume (V)	1318.5 (11) $Å^3$
Density (Dx)	1.780 Mg/m^3
Wavelength (λ)	0.71073 Å
Data collection instrument	Bruker APEX-II CCD diffractometer
Radiation	Mo Kα (λ = 0.71073 Å)
θ Max	28.7°
θ Min	2.8°
θ Range	2.8°–28.0°
Total reflections	31,584
Independent reflections	6622
Reflections with $I > 2\sigma(I)$	5014
Absorption correction	Multiscan
Rint	0.083
Crystal dimensions	0.15 × 0.11 × 0.10 mm
Temperature (T)	110 K
Hydrogen site location	Inferred from neighboring sites, H atoms constrained
Refinement method	Least squares refinement on F2
R ($F2 > 2\sigma(F2)$)	0.052
wR (F2)	0.117
S (goodness of fit)	1.06
Number of parameters	318
Restraints	None
Maximum electron density (ρmax)	1.18 $e/Å^3$
Minimum electron density (ρmin)	−1.97 $e/Å^3$
(Δ/σ)max	0.001
Absorption coefficient (μ)	5.63 mm^{-1}
θmax	28.7°
θmin	2.8°

2.3 | Biological Assessment

2.3.1 | Preparation of Monomeric $A\beta_{(1–42)}$ and Complexes Stock Solutions

Commercially purchased $A\beta_{(1–42)}$ first interacted with HFIP, resolved, and published in accordance with the literature. Again, the literature was used to determine the concentration according to itseffects [66]. Then, solutions were prepared so that the DMSO/H_2O and DMSO ratio did not exceed 1%. Due to the low water solubility of the complexes, the complexes for the prepared stock solution were dissolved in 2:1 DMSO/H_2O medium and diluted to the targeted concentrations with phenol-free DMEM (Dulbecco's Modified Eagle Medium).

2.3.2 | Cell Culture Studies

Human neuroblastoma cancer cell (SH-SY5Y) was used in cell culture studies. After removing the frozen cell from −80°C in the cryotube, then it was quickly thawed in a water bath and transferred to a flask, andflask, and filled with DMEM medium. Phenol-red-free DMEM was selected as the medium used to determine the cytotoxicity levels of the cells, and all procedures were carried out under sterile conditions. The DMEM medium was prepared with 1% penicillin/streptomycin, 1% L-Glutamine, 1% nonessential amino acid, and 1% Sodium-pyruvate added to the bottlebottle, and it was completed to 500 mL. For an optimal environment for cell growth, the cells were kept in an incubator at 37°C, containing 95% humidity and 5% CO_2 conditions.

2.3.3 | Cytotoxicity Studies

In 96-well plates, 1×10^5 SH-SY5Y cells (for 72 h) were seeded in each well. To determine the cytotoxicity of the complexes alone, master stock solutions of the complexes were diluted with DMEM to the obtained concentrations and added to the wells at (0.1; 0.5; 1; 10; 50; 100) μM concentrations. After 72 h of cell cultivation, the medium was removed from the cells and the wells were washed two times with 1× PBS. At the end of the relevant time, the medium was removed from the cells; 100 μL of 0.5 mg/mL MTT was added to each well and incubated at 37°C for 3 h. After the incubation was completed, the medium with MTT was removed from each well and 150 μL of DMSO was added to dissolve the MTT crystals in the cell. The absorbance of the wells was measured at 570 nm with a microplate reader (Thermo Scientific, Varioskan Flash). The percent viability of the control group (untreated group) was considered 100%, and the absorption value of each well was calculated as a percentage relative to the control group, and the experiments were repeated three times. As a result of this study, the inhibitory effect of the complexes on the toxicity of $A\beta_{1-42}$ in neuronal cell culture was determined by MTT measurement. Neuronal cells were incubated with $A\beta_{1-42}$ for 72 h (Interaction with HFIP may give erroneous results for the first 24 h) [67] with a final concentration of 10 μM in the presence of complexes at concentrations of 10 and 5 μM, respectively. After removing the medium from the installation, 0.5 mg/mL MTT was added to the wells and incubated at 37°C for 3 h. After the incubation period was completed, the medium with MTT was removed from each well, and 150 μL of DMSO was added to open the MTT crystal cells inside. The absorbance of the wells was measured at 570 nm with a microplate reader and again compared with the control group to calculate the percentage of cell viability [68].

2.3.4 | MALDI TOF Mass Spectrometry

$A\beta_{1-16}$ was used for Maldi-TOF MS measurements. The stock solutions prepared from $A\beta_{1-16}$ and complexes correspond to a 1.0:1.0 M ratio. $A\beta_{1-16}$ stock solution was prepared by diluting with H_2O in PBS buffer to a final concentration of 50 μM. Mass measurements were taken from the prepared samples during a 6-h incubation period. They were incubated at 37°C. Our sample was combined with HCCA matrix as 1:3 (2:6 μL), and measurements were taken with Maldi-TOF/MS Bruker Daltonik Autoflex III spectrophotometer.

2.3.5 | AFM Measurements

Interactions of complexes with $A\beta_{(1-42)}$ In AFM measurements; $A\beta_{1-42}$ stock solution was diluted with PBS volume determined final concentrations (amyloid/complex at 1.0:1.0 and 1.0:0.5 M ratio), and the complexes were diluted with H_2O to reach the desired concentrations. For a 1.0:1.0 M ratio, 50 μM $A\beta_{1-42}$ was prepared corresponding to 50 μM complex and incubated at 37°C for 48 h. At the end of incubation, complex/amyloid samples were taken and spread on transparent coverslips and dried. Images of the dried samples were recorded with the BRUKER Dimension Edge with ScanAsyst device.

2.3.6 | Thioflavin T Assay

$A\beta_{(1-42)}$ Aggregation Kit was purchased from AnaSpec. The concentrations were prepared according to the kit procedure. For this purpose, stock solutions of complexes and $A\beta_{1-42}$ prepared as specified in the biological measurements above were diluted with buffer containing 50 mM Tris/150 mM NaCl, 20 mM HEPES/ 150 mM NaCl, 10 mM Phosphate/150 mM NaCl, and final concentrations 10 μM for $A\beta_{1-42}$ and 10 μM for the complexes (corresponding to an interaction ratio of 1:1 and 0.5:1) were prepared. The final DMSO concentration does not exceed 1%. ThT solution prepared with buffer was adjusted to the final concentration of 42.6 μM. It was determined by the literature data that an effective signal was obtained at this concentration [69]. Negative controls consisting of ThT and assay buffer and also consisting of ThT complexes (Ia, III, and IV) were run to ensure that complex does not alter ThT fluorescence. Samples were plated in a black 96-well plate. The plate was sealed with aluminum sheets to prevent samples from light and kept in the dark. Fluorescence was measured through the plate bottom every 5 min for 165 min at excitation 440 nm and emission 484 nm on a Thermo Fisher Scientific, Varioskan Flash microplate reader. Samples were kept at 37°C under orbital agitation (550 rpm) in the plate reader between reads. Kinetic was plotted using GraphPad Prism.

2.4 | Synthesis

2.4.1 | Synthesis of Ligands

2.4.1.1 | 2-(4-(Benzyloxy)-3-Methoxyphenyl)-1-Phenyl-1H-Benzimidazole (L I). A solution of 4-benzyloxy-3-methoxybenzaldehyde (0.132 g, 0.544 mmol) was prepared in 3-mL DMF medium. To this solution, N-phenyl-ortho-phenylenediamine (0.100 g, 0.544 mmol) solution in DMF (2 mL) medium was added dropwise. $Na_2S_2O_5$ was used as the catalyst. It was stirred at reflux temperature for 24 h. At the end of the reaction, cold water was added to the medium. The precipitated cream colored solid was filtered using a particle funnel. The solid part was crystallized with DCM/diethyl ether, and the product was obtained. Yield: 75%, melting point: 138°C–140°C. FT-IR (KBr disk, cm^{-1}): υ Ar-H –C=N: 3423–2880.

^{1}H-NMR (400 MHz, $CDCl_3$) ppm: 7.81 (dt, 1H, J1 = 8.0 Hz, Ar-H), 7.48–7.15 (m, 14H, Ar-H), 6.99 (dd, 1H, J1 = 8.4 HzJ2 = 2 Hz Ar-H), 6.72 (d,1H, J = 8.4 Hz, Ar-H), 5.07 (s, 2H, O-CH_2), 3.64 (s, 3H, O-CH_3) ^{13}C-NMR (100 MHz, $CDCl_3$) δ (ppm): 152.2, 149.2, 149.1, 142.9, 137.3, 136.6, 129.9, 128.6, 128.5, 128.0, 127.6, 127.3, 123.1, 122.9, 122.8, 122.4, 119.6, 113.1, 112.8, 110.3, 70.8, 55.6. Elemental analysis (%) = ($C_{27}H_{22}N_2O_2$) (406.48); calculated; C, 79.78; H, 5.46; N, 6.89; found; C, 79.69; H, 5.37; N, 7.00.

2.4.1.2 | (N1-(4-(Benzyloxy)-3-Methoxybenzylidene)-N2-Phenylethane-1,2-Diamine) (L II). Methanol (4 mL) solution of 4-Benzyloxy-3-Methoxybenzaldehyde (0.192 g, 0.790 mmol) and methanol (2 mL) solution of N-phenylethylenediamine (0.0107 g, 0.790 mmol) were prepared separately. These solutions were mixed and strirred for 24 h. The product formed at the end of the reaction was dried under vacuum, and a light yellow oil product was obtained. Yield: 86.3% FT-IR (KBr disk, cm^{-1}) υ C=*N* = 1642. ^{1}H (400 MHz, DMSO-d6) δ (ppm): 8.22(s,1H, CH=N), 7.45–7.36(m, 6H, Ar-H), 7.20(d, 1H, J = 7.6 Hz, Ar-H), 7.08–7.04(m, 3H, Ar-H), 6.61(d,2H, J = 8.8 Hz, Ar-H), 6.52(t, 1H, J = 7.4 Hz, Ar-H), 5.57(t, 1H, J = 5.8 Hz, N-H), 5.10(s, 2H, O-CH_2), 3.78 (s, 3H, O-CH_3), 3.71 (t, 2H, J = 5.2 Hz, N-CH_2). 3.33–3.28(m, 2H, N-CH_2).^{13}C NMR (100 MHz, DMSO-d6) δ (ppm): 161.8, 150.6, 149.8, 149.3, 137.2, 130.0, 129.4, 128.9, 128.4, 128.3, 123.0, 116.2, 113.2, 112. 7, 109.9, 70.4, 60.1, 55.8, 44.4. Elemental analysis (%) = ($C_{23}H_{24}N_2O_2$) (360.45); calculated; C, 76.64; H, 6.71; N, 8.88; found; C, 76.23; H, 6.79; N, 8.94.

2.4.1.3 | 2-(3-Phenoxyphenyl)-1-Phenyl-1H-Benzimid azole (L III). The synthesis of this ligand was carried out according to the literature data, and the route given for the L1 ligand was applied [57]. A solution of 3-phenoxybenzaldehyde (0.108 g, 0.542 mmol) was prepared in 2 mL DMF medium. N-phenyl-ortho-phenylenediamine (0.100 g, 0.542 mmol) solution in DMF (2 mL) medium was added dropwise, and $Na_2S_2O_5$ was added as a catalyst. It was stirred at reflux temperature for 6 h. At the end of the reaction, cold water was added to the medium. The precipitated cream colored solid was filtered using a particle funnel. The solid part was crystallized with DCM/diethyl ether, and the product was obtained. Yield: 60%, melting point: 141°C–142°C. FT-IR (KBr disk, cm^{-1}): υ Ar-H –C=N: 3398–2915. ^{1}H-NMR (400 MHz, CDCl3) δ ppm:7.87(dt, 1H, J1 = 8.4 Hz, J2 = 0.8 Hz, Ar-H), 7.49–7.00(m,15H, Ar-H), 6.86(d,2H, J = 7.6 Hz, Ar-H) ^{13}C -NMR (100 MHz, $CDCl_3$) δ (ppm): 157.2, 156.5, 151.8, 142.9, 137.2, 136.8, 131.6, 129.9, 129.8, 128.6, 127.3, 124.3, 123.5, 123.1, 119.9, 119.3, 119.1, 11 0.5. Elemental analysis (%) = ($C_{25}H_{18}N_2O$) (362.42); C, 82.85; H, 5.01; N, 7.73; found; C, 82.05; H, 5.09; N, 7.80.

2.4.1.4 | (N1-(4-(Benzyloxy)benzylidene)-N2-Phenylethane-1,2-Diamine) (LIV). The synthesis of this ligand was carried out according to the literature data, and the route given for the L1 ligand was applied [58]. 4--benzyloxybenzaldehyde (0.167 mg, 0.790 mmol) solution was prepared in methanol (3 mL) medium. Then, N-phenylethylenediamine (0.107 g, 0.790 mmol) solution in 2 mL methanol was added slowly and stirred at room conditions for 24 h. A precipitate formed in the reaction after 24 h. The precipitated material was separated by filtration. The crude sample was purified by crystallization with dichloromethane/diethyl ether and dried under vacuum. Yield: 87.5%, FT-IR (KBr disk, cm^{-1}) υ C=*N* = 1642. ^{1}H NMR (400 MHz, DMSO-d6) δ (ppm): 8.25(s,1H, CH=N), 7.69(d, 2H, J = 8.4 Hz, Ar-H), 7.46(d, 2H, J = 7.2 Hz, Ar-H), 7.39(t, 2H, J = 7.4 Hz, Ar-H), 7.09–7.05 (m, 4H, Ar-H), 6.62(d,2H, J = 8.0 Hz, Ar-H), 6.53(t, 1H, J = 7.2 Hz, Ar-H), 5.57(t, 1H, J = 6.0 Hz, N-H), 5.15(s, 2H, O-CH_2), 3.71 (t, 2H, J = 6.2 Hz, N-CH_2), 3.32–3.28(m, 2H, N-CH_2). ^{13}C NMR (100 MHz, DMSO-d6) δ (ppm): 161.5, 160.7, 149.2, 137.2, 129.9, 129.6, 129.3, 128.9, 128.4, 128.2, 116.1, 115.3, 112.6, 69.8, 60.0, 44.3. Elemental analysis (%) = ($C_{22}H_{22}N_2O$) (330.42); calculated; C, 79.97; H, 6.71; N, 8.48; found; C, 79.69; H, 6.57; N, 8.23.

2.4.2 | Synthesis of Complexes

2.4.2.1 | Synthesis of [PtCI$_2$(DMSO)(LI)], (Ia). In complex synthesis, L I (0.0289 g, 0.0710 mmol) was dissolved in 3 mL of chloroform medium. Then, Pt $(DMSO)_2Cl_2$ (0.0300 g, 0.0710 mmol) was prepared as suspended in 3 mL of chloroform medium in a test tube and added dropwise onto LI. Then the mixture was stirred at room conditions for 2 h. The solvent was evaporated in vacuo. The solid fraction was washed with diethylether and dried in vacuo. The trans structure product was obtained. Yield: 47%. Melting Point: 241°C–265°C decomposition. FT-IR (CsI disk, cm^{-1}): υ Ar-H –C=N: 3423–2880, υ S-O = 1122, υ Pt-Cl = 325.74. ^{1}H-NMR (400 MHz, CDCl3) δ (ppm): 8.40(d, 1H, J = 8.4 Hz, Ar-H), 7.73(s,1H, Ar-H), 7.51–7.23(m,14H, Ar-H), 6.86 (d,1H, J = 8.4 Hz, Ar-H), 5.15 (s,2H, O-CH_2), 3.84 (s,3H, O-CH_3) 3.40 (s,6H, O-S- $(CH_3)_2$), ^{13}C-NMR (100 MHz, $CDCl_3$) δ (ppm): 150.2, 149.1, 139.2, 136.3135.1, 130.0,129.4, 128.6, 128.1, 127.5, 127.3125.1, 124.8, 124.2, 11 9.1, 114.6, 112.6, 111.1, 70.8, 56.2, 43.7. Elemental analysis (%) = ($C_{29}H_{28}Cl_2N_2O_3PtS$) (750.59); calculated C, 46.40; H, 3.76; N, 3.73, found; C, 46.45; H, 3.72; N, 3,76.

2.4.2.2 | Synthesis of [PtCI$_2$(DMSO)(LI)], (Ib). In complex synthesis, Complex Ia was refluxed in CH_3CN medium for 4 days. The small amount of solid formed was separated. The filtrate was evaporated in vacuo. The solid formed was washed with diethylether and dried in vacuum. Cream colored product was obtained. Yield: 40% Melting Point: 174°C–196°C decomposition. FT-IR (CsI disk, cm^{-1}): υ Ar-H –C=*N* = 3423–2880, υ S-O = 1122, υ Pt-Cl = 325.51. ^{1}H-NMR (400 MHz, $CDCl_3$) δ (ppm): 8.38(d, 1H, J = 8.4 Hz, Ar-H), 7.97(s,1H, Ar-H), 7.50–7.21(m,14H, Ar -H), 6.88 (d, 1H, J = 8.4 Hz, Ar-H), 5.26 (s, 2H, O-CH_2), 3.92 (s, 3H, O-CH_3), 3.29 (s, 3H, O-S- (CH_3), 2.46(s,3H, O-S-(CH_3), ^{13}C-NMR (100 MHz, $CDCl_3$) δ (ppm): 149.9, 149.4, 136.1, 135.0, 130.0, 129.5, 128.7, 128.2, 127.3, 125.4125.1, 124.1, 119.1, 119.0, 115.4, 112.9111.2, 70.6, 56.7, 44.3, 43.7,29.7. Elemental analysis (%) = ($C_{29}H_{28}Cl_2N_2O_3PtS$) (750.60); calculated; C, 46.40; H, 3.76; N, 3.73 found; C, 46.36; H, 3.80; N, 3,77.

2.4.2.3 | Synthesis of [PtCI$_2$(DMSO)(LII)], (II). In complex synthesis, L II (0.0494 g, 0.137 mmol) was dissolved in 3 mL of chloroform medium. Pt $(DMSO)_2Cl_2$ (0.0580 g, 0.137 mmol) was prepared as suspension in 4 mL of chloroform medium and added dropwise onto LII. The mixture was then refluxed for 72 h. At the end of the reaction, the solvent was concentrated in the vacuum line until 1 mL of solution volume remained and a light yellow solid was obtained by precipitation with 5 mL of diethylether. The product was filtered and dried under a vacuum. Yield: 65%, Melting Point: 115°C, FT-IR (CsI disk, cm^{-1}) υ C=*N* = 1598 υ

Pt-Cl = 321. ^{1}H NMR (400 MHz, DMSO-d6) δ (ppm): 9.15 (s,1H, CH=N), 7.67–7.18(m, 13H, Ar-H), 5.19(s, 2H, -CH2), 4.14 (bs, 1H, N-CH_2),3.95–3.83(m, 1H, N-CH_2), 3.82 (s, 3H, O-CH_3), 3.04(bs, 1H, N-CH_2),2.75(bs, 1H, N-CH_2).^{13}C NMR (100 MHz, DMSO-d6) (ppm): 171.3, 152.5, 148.9, 148.3, 137.7, 129.8, 129.5, 129.0, 128.5, 127.3, 124.1, 116.9, 113.2, 112.8, 112.5, 70.4, 60.5, 56.1, 46.1. Elemental analysis (%): calculated ($C_{23}H_{24}Cl_2N_2O_2Pt$) (626.44) C, 44.10; H, 3.87; N, 4.47; found, C, 43.56; H, 4.52, N, 4.01.

2.4.2.4 | Synthesis of [$PtCI_2$(DMSO) (L III)], (III). This complex synthesis was carried out according to literature data [57]. In complex synthesis, L III ligand (0.0300 g, 0.0828 mmol) was dissolved in 3 mL of chloroform medium. Then, Pt $(DMSO)_2Cl_2$ (0.0349 g, 0.0828 mmol) suspension prepared in 3 mL of chloroform medium in a test tube was added dropwise onto L III. Then the mixture was stirred at room conditions for 4 days. At the end of the reaction, the solvent was dried under vacuum. The resulting solid part was first washed with acetone. The insoluble fraction was separated. The solvent was evaporated in vacuo and washed with diethylether. Yield: 72% Melting Point: 232°C. FT-IR (CsI disk, cm^{-1}): υ Ar-H- (–C=N): 3398–2915, υ S-O = 1121, υ Pt-Cl = 319.13. ^{1}H-NMR (400 MHz, CDCl3) δ (ppm): 8.41(d, 1H, J = 8.4 Hz, Ar-H), 8.03(d, 1H, J = 7.6 Hz, Ar-H), 7.56–7.45 (m, 5H, Ar-H), 7.37(t,2H, J = 7.8 Hz, Ar-H), 7.31–7.20(m, 7H, Ar-H), 7.11(t, 1H, J = 6.8 Hz, Ar -H), 6.83(d, 2H, J = 8.8 Hz, Ar-H), ^{13}C-NMR (100 MHz, $CDCl_3$) δ (ppm): 157.0, 155.7151.6, 139.5, 134.5, 130.2130.1130.0, 129.5129.0, 127.2, 126.3, 125.6, 125.1, 124.0, 121.5, 120.7, 119.4, 119.0, 111.3, 77.0, 76.6, 44.6, 43.8. Elemental analysis (%) = ($C_{27}H_{24}Cl_2N_2O_2PtS$) (706.53); calculated; C, 45.90; H, 3.42; N, 3.96, found; C, 45.73; H, 3.48; N, 4.02.

2.4.2.5 | Synthesis of [$PtCI_2$(DMSO)(LIV)] (Complex IV). This complex synthesis was carried out according to literature data [58]. In complex synthesis, L IV (0.0453 g, 0.137 mmol) was dissolved in 2 mL of chloroform medium. Pt $(DMSO)_2Cl_2$ (0.0580 g, 0.137 mmol) was prepared as suspension in 3 mL of chloroform medium and added dropwise onto LIV. The mixture was then refluxed for 72 h. At the end of the reaction, the reaction mixture was concentrated in a vacuum line until 1 mL of solution volume remained and was precipitated with 5 mL of diethylether to obtain a light yellow solid. The product was filtered and dried under a vacuum. Yield: 61%, Melting Point: 197°C decomposition, FT-IR (CsI disk, cm^{-1}) υ C=*N* = 1599, υ Pt-Cl = 328, ^{1}H NMR (400 MHz, DMSO-d6) δ (ppm): 9.14 (s,1H, CH=N), 7.79–7.15(m, 13H, Ar-H), 5.51(d, 1H, -NH), 5.20 (s, 2H, -CH2), 4.09 (bs, 1H, N-CH_2), 3.92(bs, 1H, N-CH_2), 3.03 (bs, 1H, N-CH_2), 2.77(bs, 1H, N -CH_2). ^{13}C NMR (100 MHz, DMSO-d6) δ (ppm): 165.8, 161.5, 146.5, 133.1, 129.4, 129.0, 128.3, 124.5, 124.3, 124.0, 115.8, 115.3, 112.5, 70.0, 61.08, 60.1, 46.0. Elemental analysis (%): calculated ($C_{22}H_{22}Cl_2N_2OPt$) (596.41) C, 44.30; H, 3.72; N, 4.70; found, C, 43.81; H, 4.18, N, 4.28.

3 | Results and Discussion

3.1 | Synthesis and Spectroscopic Studies

The ligand and the synthesized complexes in the study are shown in Scheme 1.

The synthesized ligands and complexes are shown in Scheme 1. In this study, the first step was to synthesize the ligands LI and

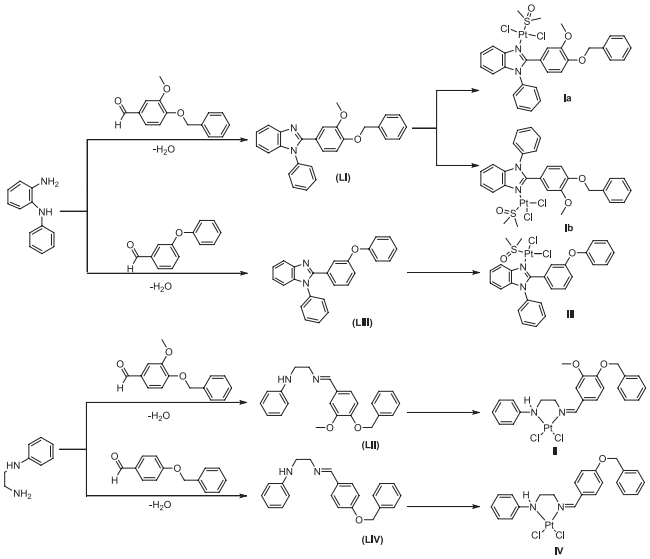

SCHEME 1 | Synthesis of ligand and complexes.

LII, which are benzimidazole and schiff bases consisting of the same aldehyde and two different amines. The other 2 ligands (LIII and LIV) were synthesized analogously to these. The aldehydes and amines used have aromatic groups, and it was thought that their passage through the SH-SY5Ycell membrane would be facilitated [70]. The FT-IR, ^{1}H NMR, and ^{13}C NMR spectra of the synthesized ligands L I and L II are provided in the supporting information (S1–S6). Additionally, the spectra of the L III and L IV, which were previously reported, have also been included in the supporting information (S7, S8, S9 and S10, S11, S12). The ^{1}H NMR spectra for the ligands (Ligand I, Ligand III) were recorded in $CDCl_3$, while those for L II and L IV were obtained in DMSO-d_6. The FT-IR spectra were recorded using KBr pellets.

In the FT-IR spectrum of the L I, bands corresponding to Ar-H stretching vibrations are observed above 3000 cm^{-1}, while aliphatic C-H stretching vibration bands are found below 3000 cm^{-1}. In the ^{1}H-NMR spectrum, peaks corresponding to Ar-H are seen in the range of 6.73–7.81 ppm. A peak related to the O-CH_3 group is observed at 3.64 ppm. The protons of the O-CH_2 group attached to the C2 carbon appear as a singlet at 5.07 ppm. The ^{13}C-NMR spectrum also supports the structure. Elemental analysis data are consistent with the proposed structure.

The vibration mode related to the imine group for ligand II was observed at 1642 cm^{-1} in the FT-IR spectrum. Again, it was observed that the –CO group vibration related to the aldehyde disappeared for ligand II. In the ^{1}H-NMR spectrum of LII, the peak related to the H of the imine group was observed as a singet at 8.22 pm, and in the ^{13}C-NMR spectrum of ligand II, the imine C was observed at 161.8 ppm. The peak for the –OCH_3 group in Ligand II is located at 3.78 ppm. The ^{1}H-NMR, ^{13}C-NMR, and FT-IR values obtained for Ligand II also support the proposed structure.

Since there are only aromatic groups in the Ligand III, the explanation given for ligand I in the FT-IR spectrum is valid, and ring skeleton vibrations are seen in the 700–800 cm^{-1} region. In the ^{1}H-NMR spectrum, peaks belonging to hydrogens attached to the aromatic ring are seen in the range of 6.86–7.87 ppm. Again, in the ^{13}C-NMR spectrum, there are

peak groups related to carbon atoms that are compatible with the structure.

In ^{1}H-NMR for L IV, the hydrogen bonded to the imine carbon is seen as a singlet at 8.25 ppm. In the FT-IR spectrum, the vibration mode related to the imine group was observed at 1644 cm^{-1}, while the vibration related to the –CO group of the aldehyde was found to have disappeared [71]. Spectrum evaluation supports the formation of the expected structure for this ligand.

Complex Ia is a trans structure complex obtained by the reaction of L I with Pt $(DMSO)_2Cl_2$ in chloroform medium, while the geometric isomer cis structure complex Ib was obtained by heating this complex in CH_3CN medium. The FT-IR, ^{1}H-NMR, and ^{13}C-NMR spectra of the complexes Ia and Ib (S13, S14, S15 and S16, S17, S18) are given in the supporting information, respectively.

The structure determination studies of the product obtained as a result of the synthesis between the ligand I and the starting complex Pt $(DMSO)_2Cl_2$ in chloroform medium and at room conditions showed that the starting Pt complex, which was initially cis structured, transformed into trans (Ia) structure in the interaction with the Ligand I. Moreover, the same experiment was performed using an ice bath and produced similar results. Again, when the reaction was repeated in chloroform medium with heating (approximately 50°C), a mixture of cis and trans-structured products was obtained. In the ^{1}H-NMR spectrum of the complex Ia, it was observed that all peaks shifted to the weak field compared to the free ligand. The hydrogen atoms at the peak of the dmso group bound to Pt (II) are located at 2.46 and 3.29 ppm, with 3 protons each. This supports the transformation of the structure to the trans state. In fact, the distinctive peak group in the FTIR spectrum of complex Ia is the Pt-CI stretching vibrations, and these vibrations, which are not present in the free ligand, were observed as a single peak at 325.7 cm^{-1} in the spectrum of complex Ia. Elemental analysis data also showed that the ligand I is monodentately bound to Pt.

In order to investigate the change in structure, some experiments were carried out on the trans-structured complex Ia, and as a result, the cis structured product (Ib) could be obtained by refluxing this complex in acetonitrile for 3 days. Although there was no significant change in the ^{1}H-NMR spectrum of this product compared to the trans structure in terms of aromatic hydrogens, especially the hydrogens of the DMSO group bound to Pt were observed as a singlet with a total of 6 protons at 3.40 ppm. On the other hand, in the FT-IR spectrum of the complex Ib, the Pt-CI peaks are observed with a shoulder at 325.6 cm^{-1} as expected from the cis structure [67]. The singlet peak belonging to O-CH_2 at 5.07 ppm in the ligand is again a singlet at 5.15 ppm in Complex Ib, but shifts to 5.26–5.15 ppm as a multiplet in Complex Ia. The ^{13}C NMR spectra for both complexes are consistent with the proposed structuresIn both complexes; benzimidazole ligands (I and III) are bonded to the Pt atom via free electron pairs on the N atoms in position 3 [72]. It is expected that ligands with monodentate behavior will bind with the metal atom via the 3rd nitrogen of the benzimidazole ring [73]. During the examination of ^{1}H-NMR spectra, the presence and locations of signals belonging to the Ar-H group were emphasized to determine that the platinum atom was bound via the 3rd position of the benzimidazole ring. Indeed, the aromatic hydrogen of the benzimidazole group appears in the weakest region of the ^{1}H-NMR spectrum and has the largest shift value [74].

The $PtCl_2$(DMSO) (L III) complex was formed by the reaction of $[PtCl_2(DMSO)_2]$ with L III in chloroform at a 1:1 M ratio and was isolated as a stable solid in air. The FT-IR spectrum of complex III (S19) was recorded using a CsI pellet. The Pt-Cl stretching vibrations appear to shift to lower wavenumbers compared to the initial complex. The S–O stretching vibration of the DMSO group, bonded via sulfur, is observed at 1121 cm^{-1} [60]. In the 1H-NMR spectrum of complex III (S20), aromatic Ar-H protons were observed in the range of 6.80–7.87 ppm. Furthermore, the ^{13}C-NMR spectrum (S21) showed multiple peaks corresponding to different carbon atoms within the structure. Notably, the signals for carbons in the DMSO group appeared in the range of 44.6–43.8 ppm. The results of elemental analysis are consistent with theoretical values. A single-crystal study of complex III was also performed. Crystal data are provided in Table 1, and bond lengths and bond angles are summarized in Table 2.

Complex III is a pale yellow single crystal (Table 1). Pt-N, Pt-Cl, and C-N bond lengths (Table 2) can be compared with literature values [75]. When looked at in terms of bond angles, it can be seen that the geometry around Pt is very close to the ideal square plane. The DMSO ligand is bound at the S terminus. Cl atoms are in cis position with each other. DMSO and the LIII ligand appear to have almost the same trans effecting potency. Because Pt–Cl bonds are approximately the same length. The single crystal X-ray image of complex III is given in Figure 1.

Complexes II and IV were synthesized as a result of the reaction of ligand II and IV with the starting complex [Pt $(DMSO)_2Cl_2$]. In the FT-IR spectrum of the complex II (S22), it is seen that the imine peak is shifted compared to the free ligand by υ C=*N* = 1598 cm^{-1}. While the Pt-Cl stretching vibrations are seen as double shoulders at 335–320 cm^{-1} in the [Pt $(DMSO)_2Cl_2$] complex, the Pt-Cl stretching vibrations are seen as only containing a single shoulder at 321 cm^{-1} for complex II [67]. Consistent with this, the imine peak in the ^{1}H-NMR spectrum of the complexII (S23) is shifted from 8.22 ppm to the weaker field of 9.15 ppm, indicating a binding from the imine end. The values of the imine carbon in the ^{13}C-NMR spectrum (S24), 161.8 for ligand II and 171.3 in complex II, support the bonding from the imine. A shift was observed in the CH_2 protons in the ethylene group to which the N-phenylamino group is attached, compared to the free ligand, and the peaks of the protons in the -CH_2 group also came by

TABLE 2 | Bond lengths and bond angles of complex III.

Bond lengths (Å)		Bond angles (°)	
N1-C7	**1.330 (8)**	**C7-N1-Pt1**	**125.2 (4)**
N1-C7	1.359 (8)	N1-Pt1-Cl1	89.48 (16)
Pt1-Cl1	2.303 (2)	Cl1-Pt1-Cl2	90.77 (9)
Pt1-Cl2	2.294 (2)	N1-Pt1-S1	88.97 (16)
Pt1-N1	2.019 (5)	S1-Pt1-Cl1	178.11 (8)
Pt1-S1	2.194 (2)	N1-Pt1-Cl2	179.06 (15)

separating one by one. This also shows that there is a bonding from the amino nitrogen. The evaluation also supports that the structure is chelate-bound. The elemental analysis results also support the proposed structure.

The FT-IR spectrum of complex IV (S25) was compared with that of the ligand (S10). This comparison revealed changes in the υ (C=N) modes due to complexation. While the cis-Pt-Cl peaks of the starting complex $[PtCl_2(DMSO)_2]$ show a clear distinction, they appear as a peak with a shoulder in the FT-IR spectrum of the Pt-L complex. However, a review of the literature indicates that this distinction is not always fully observed in some cis-structured complexes [66]. The ^{1}H and ^{13}C NMR spectra of Complex IV (S26 and S27) show shifts when compared to those of the free ligand (S11 and S12). The signal of the $-CH_2$ group bound to oxygen in the ligand shifts from 5.15 to 5.20 ppm upon complexation. The proton signal of the $-CH_2$ group bound to nitrogen, observed as a singlet at 3.71 ppm in the free ligand, appears as two separate singlets at 3.92 and 4.09 ppm after complexation. Notably, the characteristic imine proton (N=CH) and imine carbon (N=CH) signals shift to higher ppm values upon complexation, confirming that the complex is imine-bound [76–78]. The peaks corresponding to the protons of the -CH2 group in the ligand spectrum also show separation. A similar shift in the -CH2 proton signals is observed in the complex spectrum relative to the free ligand. The elemental analysis results for both the ligand and the complex align with the proposed structure.

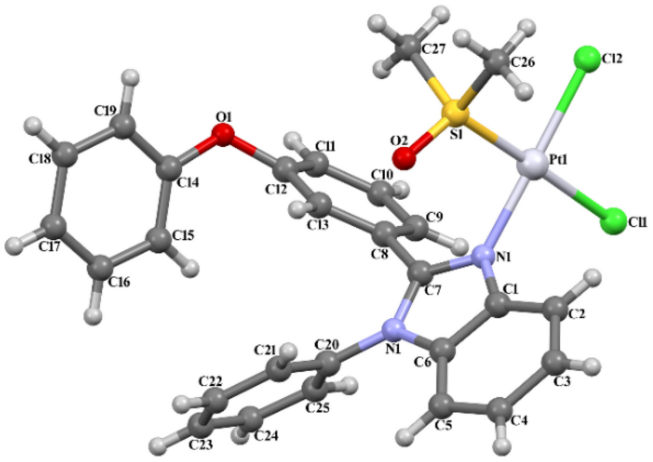

FIGURE 1 | X-ray diffraction analysis data of complex III.

3.1.1 | Cytotoxicity

The cytotoxicity of complexes Ia, Ib, II, III and IV on the SH-SY5Y cell line was examined for 72 h (Figure 2). Since there was no significant difference in the cytotoxicity values between 48 and 72 h due to studies indicating that the HFIP used in the preparation of amyloid cannot be completely removed during the process and negatively affects the interactions in the first 24 h [79], 72 h was chosen, and cytotoxicity studies were carried out during this period. The initial concentration was determined as 10 μM [51]. The range of 0.1 to 100 μM was chosen for concentrations. IC_{50} (μM) values were found to be 8.6, 2.56, 18.02, 3.73, and 19.22 μM, respectively (Table 3). This value is 18.6 μM for Cis-Pt. [75]

As can be seen from this graph (Figure 2), complexes 1b and III show very low cell viability, especially at 10 μM, which is the working concentration of amyloid [51]. Complexes Ib and III have very low IC_{50} values (2.56 and 3.73 μM, respectively). These values are well below the working concentration of 10 μM. This shows that the interaction of complexes Ib and III with amyloid on SH-SY5Y cells cannot be tested. On the other hand, complexes II and IV show high cell viability at this concentration.

Cytotoxic activities of benzimidazole-metal complexes are known [80]. As a matter of fact, they showed a similar effect on SH-SY5Y cells. There are studies in the literature [81–83] that show the relationship between the biological activities of complexes and their ligands and structural properties. In our study, benzimidazole-platinum complexes showed higher cytoxicity on SH-SY5Y cells than Schiffbaze-platinum complexes. In particular, it has been observed that the cis-structured Ib

TABLE 3 | IC_{50} (μM) values of compounds Ia, Ib, II, III, and IV.

IC_{50} (μM) values of compounds Ia, Ib, II, III, and IV					
Ia	**Ib**	**II**	**III**	**IV**	**Cis-Pt**
8.6	2.56	18.02	3.73	19.22	18.6

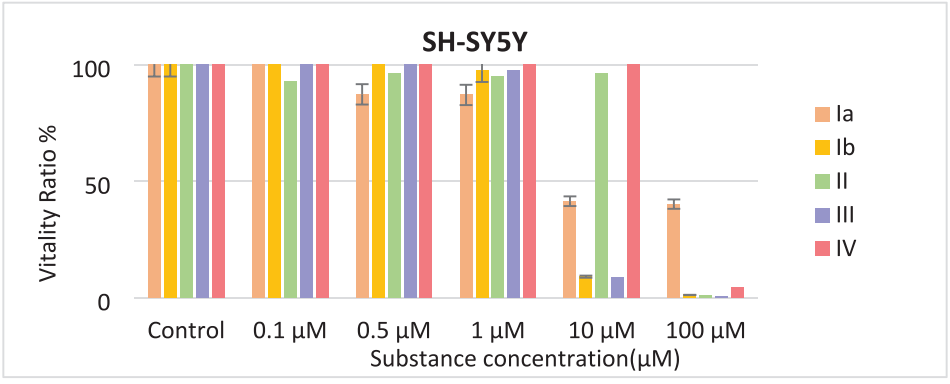

FIGURE 2 | Effects of Ia, Ib, II, III, and IV complexes on progression in SH-SY5Y cell line.

complex is much more toxic than its cis-trans-structured analog, the Ia complex. This reflects the effect of geometric isomer differentiation on cytotoxicity. Literature information also supports this conclusion [80]. It is known that especially Cl–Pt–Cl bond angles can also have an effect on cytotoxicity. In the trans-structured Ia complex, this angle is larger than in the cis-structured Ib complex, and it can be said that larger angles cause a decrease in cytotoxicity. On the other hand, the higher toxicity of benzimidazole-platinum complexes compared to Schiffbaz-platinum complexes may be related to the DMSO group in benzimidazole complexes and its interaction with cellular components.

Figure 3 shows the interaction of complexes 1a, II, and IV with SH-SY5Y cells along with amyloid. $A\beta_{1-42}$ was solely added to the medium as a control. After 72 h, 10 μM $A\beta_{1-42}$ possessed approximately 65% cell viability, which is consistent with literature data [84]. The final amyloid concentration was 10 μM, and the complex concentrations were calculated according to their ratios. The values chosen for the complex/amyloid ratio are 1:1 and 1:0.5. Because in many studies, this ratio has been measured as 2:1 or 1:1 [53, 54]. Essentially, since the complexes are expected to interact with the histidine ends of the amyloid, an interaction ratio of 1:1 is the most probable interaction. Any ratio smaller than this ratio is important as it shows the activity of the complex or low concentrations of the complexes on amyloid aggregation. Interaction with amyloid with these complexes was performed with the complex/amyloid ratio both 0.5:1 and 1:1. The Ia complex has 45% cell viability at 10 μM concentration and was used in interaction studies with amyloid with a complex/amyloid ratio of 0.5:1.

In measurements of 1:1 and 0.5:1 complex/amyloid ratio, both complexes II and IV increased cell viability. The cell viabilities found when the molar ratio was 1:1 for both complexes were higher than those found when the ratio was 0.5:1 (Figure 3). For complex Ia, the complex/amyloid molar ratio was studied as 0.5:1. Complex Ia at a 0.5:1 M ratio achieves the cell viability that complex IV at a 1:1 M ratio can provide. This ratio indicates a very low value for benzimidazole complexes [51]. In all evaluations, it is understood that the effect of benzimidazole-platinum complexes on cells is greater than Schiff base-platinum complexes, but their cytotoxic activities are more than Schiffbase-platin complexes (II and IV). Therefore, the use of benzimidazole-platinum complexes in interactions with amyloid must not exceed a certain rate. So, for complex Ia, it could only be used in interactions with amyloid with a molar ratio of 0.5:1. The molar ratios in this study are consistent with the values found for Schiff base-platinum complexes with different structures in previous studies conducted by our group [53–56, 85, 86].

3.1.2 | Thioflavine-T Aggregation İnhibition Studies

ThT, an extrinsic fluorescent dye, is able to bind to amyloid aggregates; upon binding, its fluorescence intensity increases. When fresh $A\beta_{(1-42)}$ alone was incubated at 37°C, ThT fluorescence showed a sigmoidal shape as a function of the incubation time (Figure 4).

From these graphs, it is seen that the interaction of complexes II and IV with amyloid is more as the complex/amyloid molar

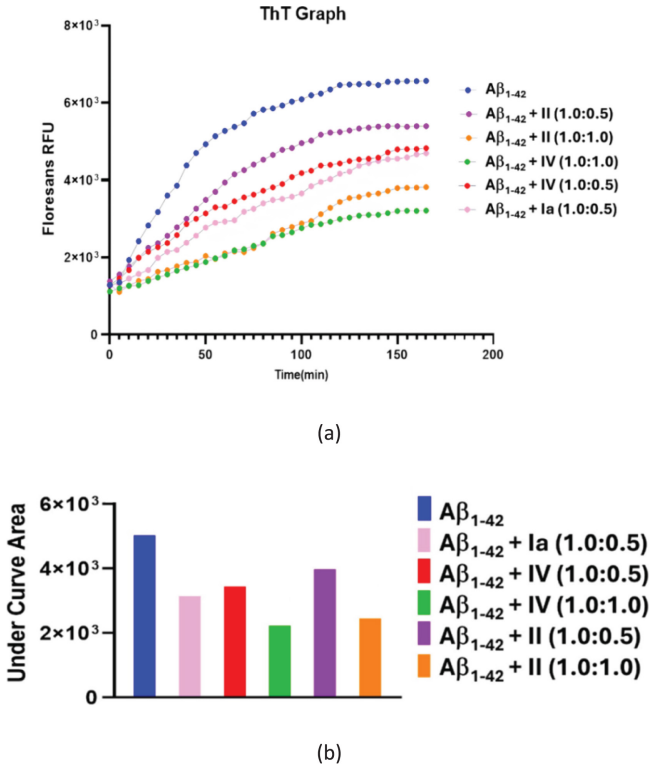

FIGURE 4 | (a) Fluorometric determination of the ability of complexes Ia, II, and IV to inhibit aggregation of the $A\beta_{1-42.}$ (b) Area under the curve area.

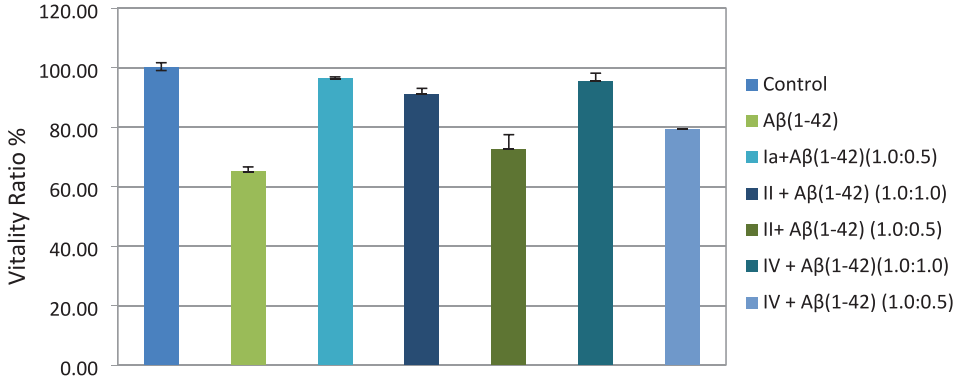

FIGURE 3 | Cell viability after the interaction between complexes with $A\beta_{1-42}$. All data represent the mean ± SEM obtained from four independent experiments. $p < 0.05$.

ratio increases. However, both complexes have the similar interaction with amyloid at a mole ratio of 1:1. In terms of mole ratios, the interactions of this ratio are more than 0.5:1. Unlike cellular data, the interaction of complex Ia with amyloid is closer to the interactions of complexes II and IV at a ratio of 0.5:1. Calculation of the area under the fluorescence curve shows that for the Ia complex, it interacts with amyloid at 40%, complex II 49% and 22% at molar ratios of 1:1 and 0.5:1, respectively. The same calculation for the IV complex shows that the interaction with amyloid is 52% and 30% at both molar ratios, respectively. The complex that interacts best at a molar ratio of 0.5:1 is complex Ia. The obtained values are comparable with the results reported for Schiff base- Pt complexes [56, 85, 86].

Kinetic data obtained from fluorescence measurements are available in the Supporting Information (S28).

The effects of Pt complexes numbered Ia, II, and IV on $A\beta_{1-42}$ aggregation were investigated at different stoichiometric ratios (1:0.5 and 1:1). The aggregation kinetics were evaluated using ThT fluorescence measurements, and the obtained kinetic data were fitted to the Boltzmann sigmoidal model using the Nonlinear Curve Fitting (NLFit) method in OriginPro software.

As a result of these analyses, the initial and maximum fluorescence intensities (A_1 and A_2), the time point at which the aggregation process begins to accelerate (x_0, lag time), the slope value indicating the aggregation rate (dx), and the R^2 coefficient of determination, which shows the model's fit to the experimental data, were calculated. The R^2 values obtained from the modeling were found to be above 0.95 in all cases, demonstrating that the model provides a high degree of fit to the experimental data.

At a 1:0.5 ratio, complex-Ia exhibited an aggregation acceleration point at $x_0 = 75.64$ min, with an R^2 value of 0.95285. The aggregation rate parameter was found to be $dx = 28.25 \pm 6.37$, indicating the rate at which the aggregation process progresses.

In studies conducted with complex-II, the aggregation acceleration point was determined as $x_0 = 36.28$ min at a 1:0.5 ratio, with an R^2 value of 0.99928. When the 1:1 ratio interaction was applied, the aggregation process started later ($x_0 = 85.88$ min), and the model's fit to the data was found to be $R^2 = 0.99031$.

For complex-IV, the aggregation acceleration point was determined as $x_0 = 61.07$ min at a 1:0.5 ratio, with an R^2 value of 0.95951. Under the 1:1 ratio, aggregation started earlier ($x_0 = 58.65$ min), but the model's fit to the experimental data remained highly accurate ($R^2 = 0.99855$).

3.1.3 | AFM Analysis

THT measurement results are supported by AFM measurements (Figure 5). In these measurements, the complex/amyloid molar ratio is 1:1, and amyloid aggregates (especially oligomers) are observed to decrease in all three complexes (Ia, II, and IV). The morphology of the aggregates was greatly changed as a result of the interaction with the complexes. AFM imaging results visualized that these complexes effectively reduced the formation of $A\beta_{1-42}$ aggregates [87].

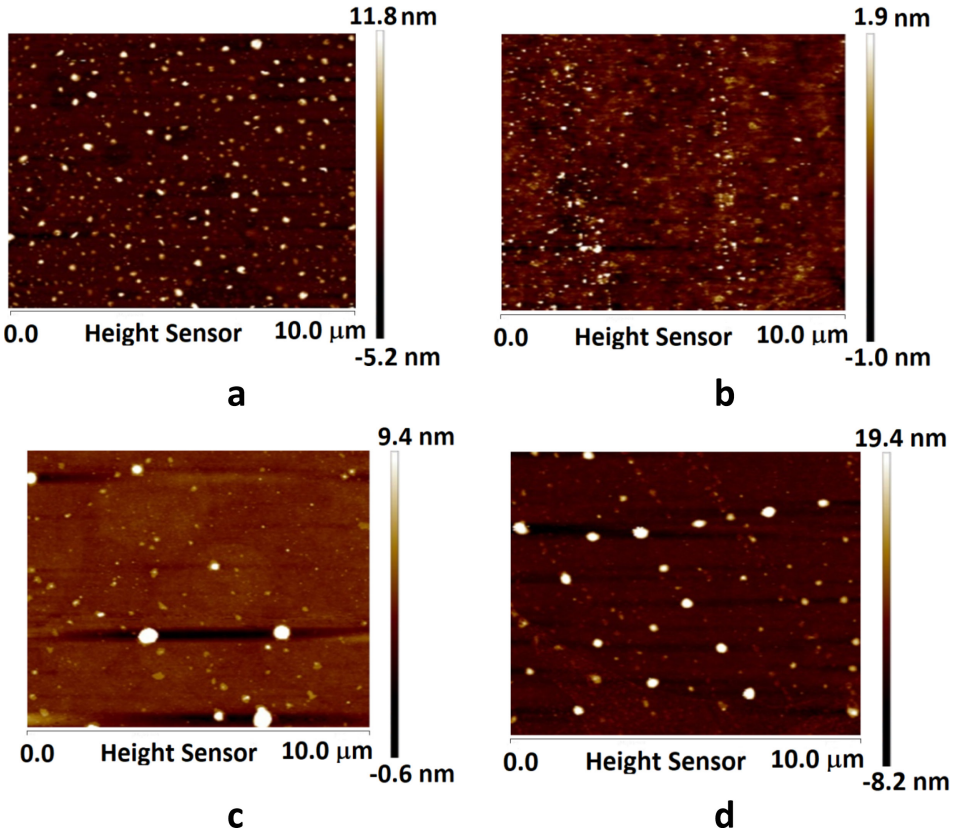

FIGURE 5 | AFM images. (a) $A\beta_{1-42}$ aggregates. (b) Ia + $A\beta_{1-42}$. (c) II + $A\beta_{1-42}$. (d)IV + $A\beta_{1-42}$.

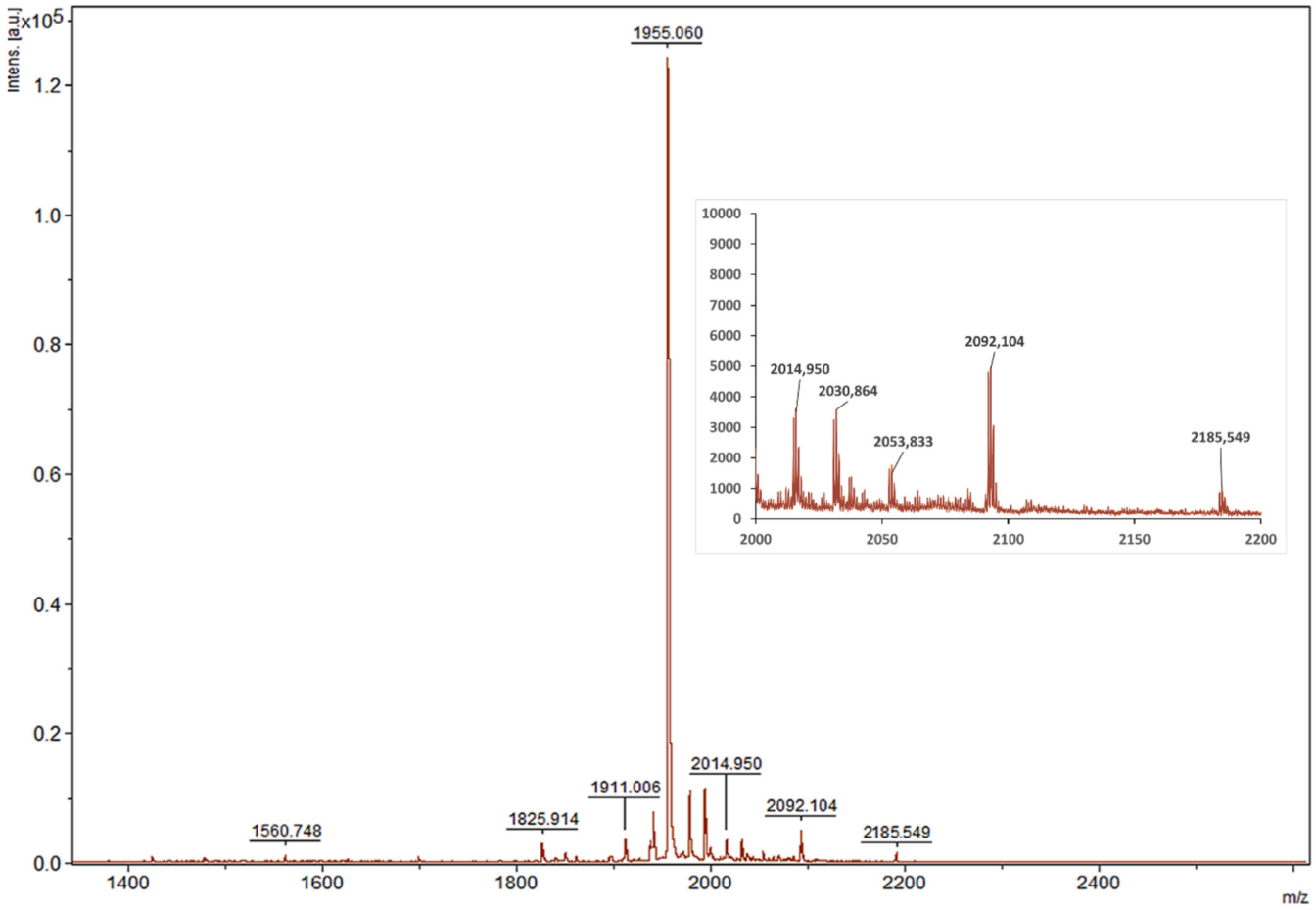

FIGURE 6 | MALDI TOF/MS spectrum of complex Ia + $A\beta_{1-16}$ interaction.

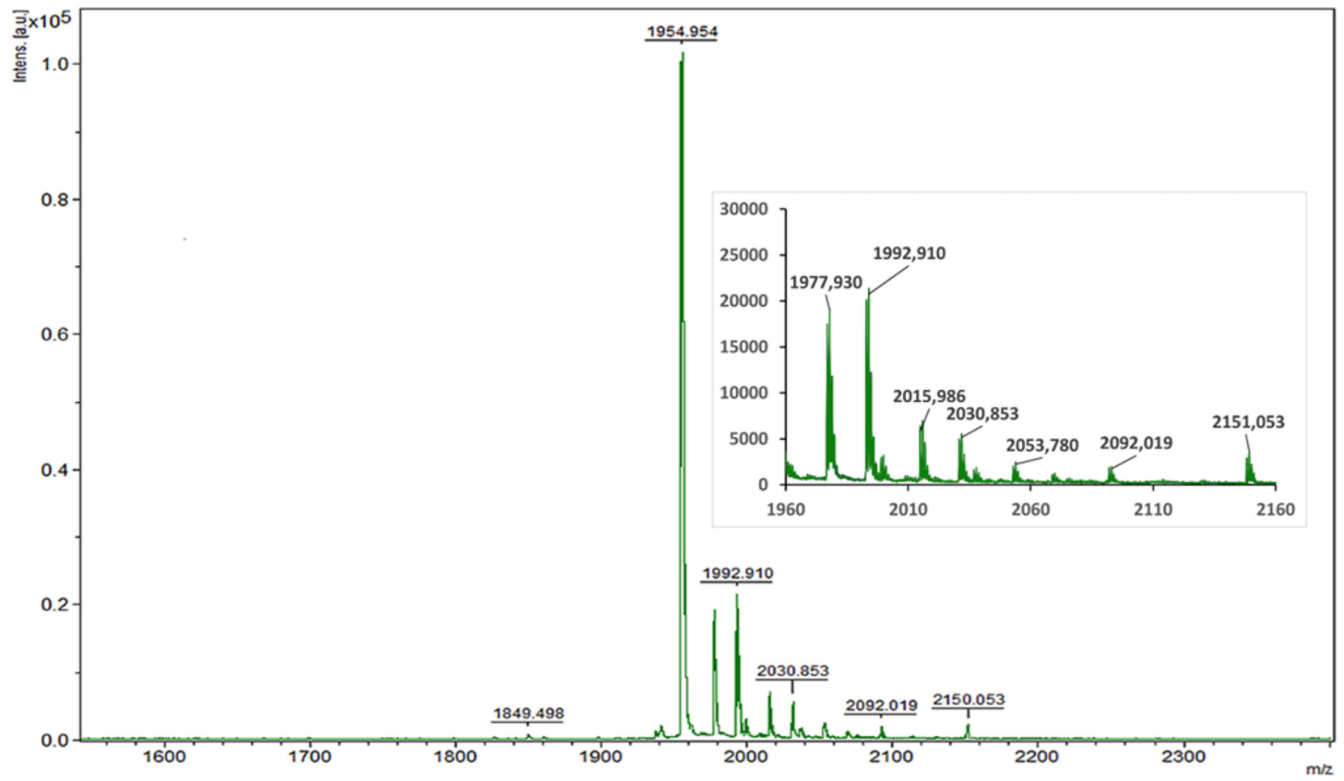

FIGURE 7 | MALDI TOF/MS spectrum of complex IV + $A\beta_{1-16}$ interaction.

3.1.4 | Maldi-TOF/MS Mass Spectrum of Interaction With $A\beta_{1-16}$

However, a peak corresponding to a mass higher than the amyloid mass, indicating interaction with $A\beta_{1-42}$, was not detected in the MALDI–TOF MS spectrum. Similar findings have been reported in the literature [76], and the situation was evaluated as if this expected peak remained in the matrix. The interactions of the complexes with $A\beta_{1-16}$, which has a smaller mass than $A\beta_{1-42}$ and contains parts of $A\beta_{1-42}$ expected to interact with metal complexes (histidine, tyrosine, etc.), were investigated by MALDI–TOF MS spectrometry [18]. Again, for this purpose, $A\beta_{1-16}$, which is a smaller structure but is an amyloid containing histidine and tyrosine groups as in $A\beta_{1-42}$, can also be used [21]. On the other hand, these complexes can also inhibit aggregation by breaking down amyloid. Both cases can be evaluated from MS spectra. As a matter of fact, MALDI Tof/MS spectra of the complexes in our study were taken with $A\beta_{1-16}$. In the incubation examination of the interaction of complexes Ia (0.5:1 M ratio), II (1:1 M ratio), and IV (1:1 M ratio) with $A\beta_{1-16}$ using MALDI TOF spectrometry, amyloid and complexes were tried to interact for 6 h of incubation. The MALDI/TOF MS spectra illustrating the interactions of Complexes Ia and IV with $A\beta_{1-16}$ are shown in Figures 6 and 7, while that of Complex II is available in the Supporting Information (S29). It has been stated in the articles that the amyloid binding regions of the complexes may be regions such as histidine and (His6,13,14) and tyrosine (tyr-10) [18, 21]. When the spectra of complexes, Ia, II, IV, are evaluated, it can be understood that the first of these interactions is encountered. The m/z values of the three complexes synthesized in this study, indicating $A\beta_{1-16}$ + complex interactions, are 2185.55 ($A\beta_{1-16}$ + Pt + Cl), respectively; 2153 ($A\beta_{1-16}$ + Pt); 2151 ($A\beta_{1-16}$ + Pt). In addition, the presence of the peak at m/z ratio 2224 in complex IV indicates the $A\beta_{1-16}$ + Pt + 2Cl interaction (Figure 7). These spectra show that the complexes bind to the histidine groups of the amyloid by dissociating the Cl- groups. Such interactions are frequently encountered in the literature [18, 56].

4 | Conclusion

This study reveals the synthesis and comprehensive characterization of novel Pt (II) complexes containing Schiff base and benzimidazole ligands, highlighting the therapeutic potential of these complexes in combating AD. In particular, complexes Ia, II, and IV exhibited the ability to potently inhibit amyloid beta ($A\beta_{1-42}$) aggregation, a critical pathological feature of AD.

Only benzimidazole-Pt complexes act more toxic towards SH-SY5Y cells than Schiff base-Pt complexes. This shows that the complexes should be used at lower concentrations. As a matter of fact, the cytotoxicity study for complex Ia was conducted only with a complex/amyloid molar ratio of 0.5:1. Additionally, cytotoxicity evaluations on SH-SY5Y neuronal cells reveal that Schiff base–Pt complexes (II and IV) in particular have a low-toxicity profile and that these complexes stand out as strong candidates in ND research. It is shown that benzimidazole complexes have the same activity at lower molar ratios than Schiff base complexes. Complex Ia at a 0.5:1 M ratio achieves the cell viability that complex IV at a 1:1 M ratio can provide.

Findings supported by advanced techniques such as Thioflavin T fluorescence analysis, AFM imaging, and MALDI-TOF mass spectrometry show that the highest inhibition is achieved at a 1:1 complex-amyloid molar ratio for schiff base complexes. AFM imaging results visualized that these complexes effectively reduced the formation of $A\beta_{1-42}$ aggregates.

The structural flexibility of the Pt (II) complexes synthesized in the study and their interaction mechanisms with amyloid peptides provide important information for innovative treatment approaches based on the metal ion hypothesis in AD. However, more comprehensive in vivo studies are required to fully understand the clinical potential of these complexes.

In conclusion, it has been revealed that the Pt (II) complexes synthesized in this study have the potential to reduce amyloid beta toxicity associated with AD and can be evaluated in future studies on the treatment of NDs. These findings provide an important basis that will shed light on the development of new therapeutic strategies for the treatment of AD.

Author Contributions

Sevil İrişli: conceptualization, validation, supervision, funding acquisition, resources, project administration, methodology, investigation, formal analysis, visualization, data curation, writing – original draft, writing – review and editing. **Salih Günnaz:** methodology, investigation, formal analysis, visualization, data curation, software, writing – original draft, writing – review and editing. **Onur Şahin:** data curation.

Acknowledgments

We would like to thank Ege University, MATAL Center for cytotoxicity measurements, and the IYTE National Mass Spectrometry Application and Research Center for MALDI/TOF MS measurements.

Conflicts of Interest

The authors declare no conflicts of interest.

Data Availability Statement

The data that support the findings of this study are available in the Supporting Information of this article.

References

1. H. Y. Liu, C. Li, and J. J. Ma, "New Vanadium and Zinc Complexes with Schiff Base Ligand N,N′-bis(3-Ethoxy-2-Hydroxybenzylidene)ethylenediamine: Synthesis, Structures, and Biochemical Properties," *Russian Journal of Coordination Chemistry* 40 (2014): 240–245.

2. P. S. Rao, C. Kurumurthy, B. Veeraswamy, et al., "Synthesis, Antimicrobial and Cytotoxic Activities of Novel 4-Trifluoromethyl-(1,2,3)-Thia diazolo-5-Carboxylic Acid Hydrazide Schiff's Bases," *Medicinal Chemistry Research* 22 (2013): 1747–1755.

3. G. G. Mohamed, M. A. O. Mohammed, B. S. Moustafa, H. F. AbdEl-Halim, and N. A. Farag, "Spectroscopic Investigation, Thermal, Molecular Structure, Antimicrobial and Anticancer Activity With Modelling Studies of Some Metal Complexes Derived From Isatin Schiff Base Ligand," *Inorganic Chemistry Communications* 141 (2022): 109606.

4. N. Singh, A. Pandurangan, K. Rana, P. Anand, A. Ahamad, and A. K. Tiwari, "Benzimidazole: A Short Review of Their Antimicrobial Activities," *International Current Pharmaceutical Journal* 1 (2012): 119–127.

5. B. Y. W. Man, H. M. Chan, C. H. Leung, et al., "Group 9 Metal-Based Inhibitors of β-Amyloid (1–40) Fibrillation as Potential Therapeutic Agents for Alzheimer's Disease," *Chemical Science* 2 (2011): 917–921.

6. M. Townsend, G. M. Shankar, T. Mehta, D. M. Walsh, and D. J. Selkoe, "Effects of Secreted Oligomers of Amyloid Beta-Protein on Hippocampal Synaptic Plasticity: A Potent Role for Trimers," *Journal of Physiology* 572 (2006): 477–492.

7. L. B. Townsend and G. R. Revankar, "Benzimidazole Nucleosides, Nucleotides, and Related Derivatives," *Chemical Reviews* 70 (1970): 389–438.

8. M. A. Santos, K. Chand, and S. Chaves, "Recent Progress in Multifunctional Metal Chelators as Potential Drugs for Alzheimer's Disease," *Coordination Chemistry Reviews* 327 (2016): 287–303.

9. M. J. Tebbe, W. A. Spitzer, F. Victor, et al., "Antirhino/Enteroviral Vinylacetylene Benzimidazoles: A Study of Their Activity and Oral Plasma Levels in Mice," *Journal of Medicinal Chemistry* 40 (1997): 3937–3946.

10. A. A. Spasov, N. I. Yozhitsa, L. I. Bugaeva, and V. A. Anisimova, "Benzimidazole Derivatives: Spectrum of Pharmacological Activity and Toxicological Properties (A Review)," *Pharmaceutical Chemistry Journal* 33 (1999): 5–243.

11. L. M. Gaetke, H. S. Chow-Johnson, and C. K. Chow, "Copper: Toxicological Relevance and Mechanisms," *Archives of Toxicology* 88 (2014): 1929–1938.

12. S. Graßmann, B. Sadek, X. Ligneau, et al., "Progress in the Proxifan Class: Heterocyclic Congeners as Novel Potent and Selective Histamine H3-Receptor Antagonists," *European Journal of Pharmaceutical Sciences* 15 (2002): 367–378.

13. E. Fernandez-Delgado, S. Estirado, A. B. Rodríguez, E. Vinuelas-Zahínos, and F. S. Luna-Giles, "Synthesis, Characterization, Crystal Structures and Cytotoxic Activity of Pt(II) Complexes With N,N-Donor Ligands in Tumor Cell Lines," *Polyhedron* 248 (2024): 116756.

14. K. Ypsilantis, T. Tsolis, A. Kourtellaris, J. M. Manos, J. C. Plakatouras, and A. Garoufis, "Synthesis, Reactivity and Characterization of Pt(ii) Complexes With N,N′ Chelating Ligands; Structure and Dimethylsulfoxide Reactivity Relationship," *Dalton Transactions* 46 (2017): 1467–1480.

15. N. A. Vyas, S. B. Singh, A. S. Kumbhar, et al., "Acetylcholinesterase and Aβ Aggregation Inhibition by Heterometallic Ruthenium (II)-Platinum (II) Polypyridyl Complexes," *Inorganic Chemistry* 57 (2018): 7524–7535.

16. A. Kumar, L. Moody, J. F. Olaivar, et al., "Inhibition of Aβ42 Peptide Aggregation by a Binuclear Ruthenium (II)−Platinum (II) Complex: Potential for Multimetal Organometallics as Anti-Amyloid Agents," *ACS Chemical Neuroscience* 10 (2010): 691–701.

17. G. Ma, F. Huang, X. Pu, et al., "Identification of [PtCl2(phen)] Binding Modes in Amyloid-β Peptide and the Mechanism of Aggregation Inhibition," *Chemistry - A European Journal* 17 (2011): 11657–11666.

18. V. S. Streltsov, V. C. Epa, S. A. James, et al., "Structural Insights Into the Interaction of Platinum-Based Inhibitors With the Alzheimer's Disease Amyloid-β Peptide," *Chemical Communications (Cambridge)* 49 (2013): 11364–11366.

19. H. Liu, Y. Qu, and X. Wang, "Amyloid β-Targeted Metal Complexes for Potential Applications in Alzheimer's Disease," *Future Medicinal Chemistry* 10 (2018): 679–701.

20. K. J. Barnham, V. B. Kenche, G. D. Ciccotosto, et al., "Platinum-Based Inhibitors of Amyloid-Beta as Therapeutic Agents for Alzheimer's Disease," *Proceedings of the National Academy of Sciences of the United States of America* 105 (2008): 6813–6818.

21. D. Valensin, C. Gabbiani, and L. Messori, "Metal Compounds as Inhibitors of β-Amyloid Aggregation: Perspectives for an Innovative Metallotherapeutics on Alzheimer's Disease," *Coordination Chemistry Reviews* 256 (2012): 2357–2366.

22. X. Wang, C. Zhang, Y. Jiao, and Z. Guo, "Inhibitory Action of Macrocyclic Platiniferous Chelators on Metal-Induced Aβ Aggregation," *Chemical Science* 3 (2012): 1304.

23. J. M. Jong, G. Kim, J. Kim, and M. H. Lee, "Strategies Employing Transition Metal Complexes to Modulate Amyloid-β Aggregation," *Inorganic Chemistry* 58 (2019): 8–17.

24. B. K. Takasaki, J. H. Kim, E. Rubin, and J. Chin, "Determination of the Equilibrium Constant for Coordination of an Amide Carbonyl to a Metal Complex in Water," *Journal of the American Chemical Society* 115 (1993): 1157–1159.

25. D. A. Sutton and C. Buckingham, "Cobalt (III)-Promoted Hydrolysis of Amino Acid Esters and Peptides and the Synthesis of Small Peptides," *Accounts of Chemical Research* 20 (1997): 357–364.

26. W. S. Chei, H. Ju, and J. Suh, "New Chelating Ligands for Co (III)-Based Peptide-Cleaving Catalysts Selective for Pathogenic Proteins of Amyloidoses," *Journal of Biological Inorganic Chemistry* 16 (2011): 511–519.

27. J. S. Derrick, J. Lee, S. J. C. Lee, et al., "Mechanistic Insights Into Tunable Metal-Mediated Hydrolysis of Amyloid-β Peptides," *Journal of the American Chemical Society* 139 (2017): 2234–2244.

28. J. M. Suh, G. Kim, J. Kang, and M. H. Lim, "Strategies Employing Transition Metal Complexes," *Inorganic Chemistry* 58 (2019): 8–17.

29. İ. Ören, O. Temiz, I. Yalçın, E. Şener, and N. Altanlar, "Synthesis and Antimicrobial Activity of Some Novel 2,5- and/or 6-Substituted Benzoxazole and Benzimidazole Derivatives," *European Journal of Pharmaceutical Sciences* 7 (1999): 153–160.

30. A. Irfan, F. Batool, S. A. Z. Naqvi, A. Islam, S. M. Osman, and A. Nocentini, "Benzothiazole Derivatives as Anticancer Agents," *Journal of Enzyme Inhibition and Medicinal Chemistry* 35 (2019): 265–279.

31. R. Çakmak, B. Ay, E. Çınar, et al., "Synthesis, Spectroscopic, Thermal Analysis and in Vitro Cytotoxicity, Anticholinesterase and Antioxidant Activities of New Co (II), Ni (II), Cu (II), Zn (II), and Ru (III) Complexes of Pyrazolone-Based Schiff Base Ligand," *Journal of Molecular Structure* 1292 (2023): 136225.

32. B. Can-Eke, M. O. Puskullu, E. Buyukbingol, and M. Iscan, "A Study on the Antioxidant Capacities of Some Benzimidazoles in Rat Tissues," *Chemico-Biological Interactions* 113 (1998): 65–77.

33. A. Patil, S. Ganguly, and S. Surana, "A Systematic Review of Benzimidazole Derivatives as Antiulcer Agents," *Rasayan Journal of Chemistry* 1 (2008): 447–460.

34. L. K. Labanauskas, A. B. Brukstus, P. G. Gaidelis, V. A. Buchinskaite, E. B. Udrenaite, and V. K. Dauksas, "Synthesis and Anti-Inflammatory Activity of Some New 1-Acyl Derivatives of 2-Methylth io-5,6-Diethoxybenzimidazole," *Pharmaceutical Chemistry Journal* 34 (2000): 353–355.

35. C. Mock, I. Puscasu, M. J. Rauterkus, G. Tallen, J. E. A. Wolff, and B. Krebs, "Novel Pt (II) Anticancer Agents and Their Pd (II) Analogues: Syntheses, Crystal Structures, Reactions With Nucleobases, and Cytotoxicities," *Inorganica Chimica Acta* 319 (2001): 109–116.

36. U. U. Janjua, M. Pervaiz, F. Ali, et al., "Schiff Base Derived Mn (II) and Cd (II) Novel Complexes for Catalytic and Antioxidant Applications," *Inorganic Chemistry Communications* 157 (2023): 111233.

37. B. Miroslaw, "Homo- and Hetero-Oligonuclear Complexes of Platinum Group Metals (PGM) Coordinated by Imine Schiff Base Ligands," *International Journal of Molecular Sciences* 21 (2020): 3493.

38. A. Kajal, S. Bala, S. Kamboj, N. Sharma, and V. Saini, "Schiff Bases: A Versatile Pharmacophore," *Journal of Catalysts* 2013 (2013): 893512.

39. A. M. Abu-Dief, R. M. El-Khatib, T. El-Dabea, et al., "Design, Synthesis, Physicochemical Characterization, Nonlinear Optical Properties, Structural Elucidation, Biomedical Studies, and DNA Interaction of Some New Mixed Ligand Complexes Incorporating

4,6-Dimethylpyrimidine Derivative and Imidazole Ligand," *Applied Organometallic Chemistry* 38 (2024): e7463.

40. O. M. I. Adly, M. Shebl, and E. M. Abdelrhman, "Polyethyleneimine Encapsulated Schiff Base Metal Complexes for Biomedical and Catalytic Applications," *Journal of Molecular Structure* 1210 (2020): 128607.

41. M. Shebl, "Mononuclear, Homo- and Hetero-Binuclear Complexes of 1-(5-(1-(2-Aminophenylimino)ethyl)-2,4-Dihydroxyphenyl)ethanone: Synthesis, Magnetic, Spectral, Antimicrobial, Antioxidant, and Antitumor Studies," *Journal of Coordination Chemistry* 69 (2016): 199–214.

42. M. Shebl, M. Saif, A. I. Nabeel, and R. R. Shokry, "New non-Toxic Transition Metal Nanocomplexes and Zn Complex-Silica Xerogel Nanohybrid: Synthesis, Spectral Studies, Antibacterial, and Antitumor Activities," *Journal of Molecular Structure* 1118 (2016): 335–343.

43. F. N. Sayed, G. G. Mohamed, and R. G. Deghadi, "Structural Characterization and Molecular Docking Studies of Biologically Active Platinum (II) and Palladium (II) Complexes of Ferrocenyl Schiff Bases," *Journal of Molecular Structure* 1278 (2023): 134904.

44. J. Cui, Y. Wang, X. Liang, et al., "Synthesis, Antimicrobial Activity, Antioxidant Activity, and Molecular Docking of Novel Chitosan Derivatives Containing Glycine Schiff Bases as Potential Succinate Dehydrogenase Inhibitors," *International Journal of Biological Macromolecules* 267 (2024): 131407.

45. E. Pedreño, A. J. López-Contreras, A. Cremades, and R. Peñafiel, "Protecting or Promoting Effects of Spermine on DNA Strand Breakage Induced by Iron or Copper Ions as a Function of Metal Concentration," *Journal of Inorganic Biochemistry* 99 (2005): 2074–2080.

46. A. Palanimurugan, A. Dhanalakshmi, P. Selvapandian, and A. Kulandaisamy, "Electrochemical Behavior, Structural, Morphological, Calf Thymus-DNA Interaction and In-Vitro Antimicrobial Studies of Synthesized Schiff Base Transition Metal Complexes," *Heliyon* 5 (2019): e02039.

47. G. Eren, E. Emerce, L. Acik, B. Aydin, and F. A. Gumus, "Novel Trans-Pt (II) Complex Bearing 2-Acetoxymethylbenzimidazole as a Non-Leaving Ligand (Trans-[Pt (AMBi)2Cl2]): Synthesis, Antiproliferative Activity, DNA Interaction, and Molecular Docking Studies Compared With Its Cis Isomer (cis-[Pt (AMBi)2Cl2])," *Journal of Molecular Structure* 1184 (2019): 512–518.

48. A. A. Helaly, A. A. El-Bindary, and S. A. Elsayed, "Synthesis and Characterization of Co (II), Ni (II), Cu (II) and Zn (II) Chelates: DFT Calculations, Molecular Docking and Biological Applications," *Journal of Molecular Liquids* 389 (2023): 122831.

49. O. A. El-Gammal, A. A. El-Bindary, A. M. Eldesoky, and I. M. Abd Al-Gader, "Synthesis, Characterization, Molecular Docking and In Vitro Antibacterial Assessments of Anthracene-Bis (Hydrazine) Thiosemicarbazide Complexes With Co (II), Ni (II), and Cu (II) Ions," *Journal of Molecular Structure* 1322 (2025): 140339.

50. A. A. A. Awadh, "Biomedical Applications of Selective Metal Complexes of Indole, Benzimidazole, Benzothiazole, and Benzoxazole: A Review (From 2015 to 2022)," *Saudi Pharmaceutical Journal* 31 (2023): 10169.

51. G. S. Yellol, J. G. Yellol, V. B. Kenche, et al., "Synthesis of 2-Pyridyl-Benzimidazole Iridium (III), Ruthenium (II), and Platinum (II) Complexes: Study of the Activity as Inhibitors of Amyloid β Aggregation and Neurotoxicity Evaluation," *Inorganic Chemistry* 54 (2015): 470–475.

52. H. Y. Khan, A. Ahmad, M. N. Hassan, Y. H. Khan, F. Arjmand, and R. H. Khan, "Advances of Metallodrug-Amyloid β Aggregation Inhibitors for Therapeutic Intervention in Neurodegenerative Diseases: Evaluation of Their Mechanistic Insights and Neurotoxicity," *Coordination Chemistry Reviews* 501 (2024): 215580.

53. M. C. Heffern, P. T. Velasco, L. M. Matosziuk, et al., "Modulation of Amyloid-β Aggregation by Histidine-Coordinating Cobalt (III) Schiff Base Complexes," *Chembiochem* 15 (2014): 1584–1589.

54. A. Iscen, C. R. Brue, K. F. Roberts, J. Kim, G. C. Schatz, and T. J. Meade, "Inhibition of Amyloid-β Aggregation by Cobalt (III) Schiff Base Complexes: A Computational and Experimental Approach," *Journal of the American Chemical Society* 141 (2019): 16685–16695.

55. K. F. Roberts, C. R. Brue, A. Preston, et al., "Cobalt (III) Schiff Base Complexes Stabilize Non-Fibrillar Amyloid-β Aggregates With Reduced Toxicity," *Journal of Inorganic Biochemistry* 213 (2020): 111265.

56. S. İrişli, S. Günnaz, Ö. Özcan, et al., "Platinum (II) Schiff Base Complexes and Their Effects on the Inhibition of Amyloid β1-42 Aggregation," *Applied Organometallic Chemistry* 38 (2024): e7540.

57. A. Arı, S. Günnaz, and S. İrişli, "Benzimidazole-Platinum Complex and Its Cytotoxic Activity on U87 Cell Lines," *Erzincan University Journal of Science and Technology* 17 (2024): 230–240.

58. Ö. Özcan, S. Günnaz, and S. İrişli, "New Schiff Base and Its Platinum Complex: Inhibition of Amyloid Aggregation," *Karaelmas Fen ve Mühendislik Dergisi* 14 (2024): 1–11.

59. V. B. Kenche, L. W. Hung, K. Perez, et al., "Development of a Platinum Complex as an Anti-Amyloid Agent for the Therapy of Alzheimer's Disease," *Chemical Society Reviews* 52 (2013): 3374–3378.

60. J. H. Price, A. N. Williamson, R. F. Schramm, and B. B. Wayland, "Palladium (II) and Platinum (II) Alkyl Sulfoxide Complexes. Examples of Sulfur-Bonded, Mixed Sulfur- and Oxygen-Bonded, and Totally Oxygen-Bonded Complexes," *Inorganic Chemistry* 11 (1972): 1280–1284.

61. G. M. Sheldrick, "SHELXL-97," *Acta Crystallographica. Section A* 64 (2008): 112–122.

62. G. M. Sheldrick, "Crystal Structure Refinement With SHELXL," *Acta Crystallographica Section C* 71 (2015): 3–8.

63. *APEX2* (Madison, Wisconsin, USA: Bruker AXS Inc., 2013).

64. C. F. Macrae, I. J. Bruno, J. A. Chisholm, et al., "WinGX and ORTEP for Windows: An Update," *Journal of Applied Crystallography* 41 (2008): 466–470.

65. L. J. Farrugia, "WinGX and ORTEP for Windows: An Update," *Journal of Applied Crystallography* 45 (2012): 49–854.

66. T. M. Ryan, J. Caine, H. D. T. Mertens, et al., "Ammonium Hydroxide Treatment of Aβ Produces an Aggregate-Free Solution Suitable for Biophysical and Cell Culture Characterization," *PeerJ* 1 (2013): e73.

67. F. Gümüş, G. Eren, L. Açık, et al., "Synthesis, Cytotoxicity, and DNA Interactions of new Cisplatin Analogues Containing Substituted Benzimidazole Ligands," *Journal of Medicinal Chemistry* 52 (2009): 1345–1357.

68. T. Mosmann, "Rapid Colorimetric Assay for Cellular Growth and Survival: Application to Proliferation and Cytotoxicity Assays," *Journal of Immunological Methods* 65 (1983): 55–63.

69. C. Xue, T. Y. Lin, D. Chang, and Z. Guo, "Thioflavin T as an Amyloid Dye: Fibril Quantification, Optimal Concentration, and Effect on Aggregation," *Royal Society Open Science* 4 (2017): 160696.

70. C. M. Chagas, S. Moss, and L. Alisaraie, "Drug Metabolites and Their Effects on the Development of Adverse Reactions: Revisiting Lipinski's Rule of Five," *International Journal of Pharmaceutics* 549 (2018): 133–149.

71. U. Dogan, Ö. Özcan, G. Alaca, et al., "Novel Benzimidazole-Platinum (II) Complexes: Synthesis, Characterization, Antimicrobial and Anticancer Activity," *Journal of Molecular Structure* 1229 (2021): 129785.

72. R. J. Sundberg and R. B. Martín, "Interactions of Histidine and Other Imidazole Derivatives With Transition Metal Ions in Chemical and Biological Systems," *Journal of Organometallic Chemistry* 518 (1974): 29–36.

73. F. Gümüş, Ö. Agül, G. Eren, et al., "Synthesis, Cytotoxic Activity on MCF-7 Cell Line and Mutagenic Activity of Platinum (II) Complexes

With 2-Substituted Benzimidazole Ligands," *European Journal of Medicinal Chemistry* 38 (2003): 473–480.

74. C. N. Ranninger, F. Zamora, L. A. Martinez-Cruz, R. Isea, and J. R. Masaguer, "Synthesis and NMR Structural Analysis of Several Ortho Palladated Complexes of Substituted Benzo-Imidazole, -Oxazole, and -Thiazole and Study of Two Polymorphic Crystals," *Journal of Organometallic Chemistry* 518 (1996): 29–36.

75. N. T. A. Ghani and A. M. Mansour, "Structural and In Vitro Cytotoxicity Studies on 1H-Benzimidazol-2-ylmethyl-N-phenyl Amine and Its Pd (II) and Pt (II) Complexes," *Spectrochimica Acta Part A: Molecular and Biomolecular Spectroscopy* 81 (2011): 529–543.

76. B. A. Miles, A. E. Patterson, C. M. Vogels, et al., "Synthesis, Characterization, and Anticancer Activities of Lipophilic Pyridinecarboxaldimine Platinum (II) Complexes," *Polyhedron* 108 (2016): 23–29.

77. A. E. Patterson, J. J. Miller, B. A. Miles, et al., "Synthesis, Characterization and Anticancer Properties of (Salicylaldiminato)Platinum (II) Complexes," *Inorganica Chimica Acta* 415 (2014): 88–94.

78. C. Shiju, D. Arish, N. Bhuvesh, and S. Kumaresan, "Synthesis, Characterization, and Biological Evaluation of Schiff Base–Platinum(II) Complexes," *Spectrochimica Acta Part A: Molecular and Biomolecular Spectroscopy* 145 (2015): 213–222.

79. R. Capone, F. Garcia Quiroz, P. Prangkio, et al., "Amyloid-β-Induced Ion Flux in Artificial Lipid Bilayers and Neuronal Cells: Resolving a Controversy," *Neurotoxicity Research* 16 (2009): 1–13.

80. I. Łakomska, "Molecular Structure and Antitumor Activity of Platinum (II) Complexes Containing Purine Analogs," *Inorganica Chimica Acta* 362 (2009): 669–681.

81. (a)M. A. El-Bindary and A. M. Fathy, "Azo Naringenin-Based Copper (II) Complex as DNA Binder: Synthesis, Spectroscopic Characterization, and Diverse Biological Potentials," *Applied Organometallic Chemistry* 38 (2024): e7460.

82. M. M. El-Zahed, M. A. Diab, A. Z. El-Sonbati, M. H. Saad, A. M. Eldesoky, and M. A. El-Bindary, "Synthesis, Spectroscopic Characterization Studies of Chelating Complexes and Their Applications as Antimicrobial Agents, DNA Binding, Molecular Docking, and Electrochemical Studies," *Applied Organometallic Chemistry* 38 (2024): 2e7290.

83. M. A. El-Bindary and A. A. El-Bindary, "Synthesis, Characterization, DNA Binding, and Biological Action of Dimedone Arylhydrazone Chelates," *Applied Organometallic Chemistry* 36 (2022): e6576.

84. J. Krishtal, O. Bragina, K. Metsia, P. Palumaa, and V. Töugu, "In Situ Fibrillizing Amyloid-Beta 1-42 Induces Neurite Degeneration and Apoptosis of Differentiated SH-SY5Y," *PLoS ONE* 24 (2017): 1.

85. S. Günnaz, E. Yıldız, A. T. Oral, F. Yurt, A. Erdem, and S. İrişli, "Schiff Base–Platinum and Ruthenium Complexes and Anti-Alzheimer Properties," *Journal of Inorganic Biochemistry* 264 (2025): 112790.

86. S. İrişli, A. Çakır, and S. Günnaz, "Synthesis of Novel Pyrimidine-Based Schiff Base Complexes: Targeting Amyloid-β Aggregation in Alzheimer's Disease," *Bioorganic Chemistry* 154 (2025): 107999.

87. W. B. Stine, Jr., K. N. Dahlgren, G. A. Krafft, and M. J. LaDu, "In Vitro Characterization of Conditions for Amyloid-β Peptide Oligomerization and Fibrillogenesis," *Journal of Biological Chemistry* 278 (2003): 11612–11622.

Supporting Information

Additional supporting information can be found online in the Supporting Information section.